



# Characterization of CuO/n-Si pn junction synthesized by successive ionic layer adsorption and reaction method

Adel H. Omran Alkhayatt<sup>1</sup> · Mustafa D. Jaafer<sup>2</sup> · Hassan Hadi Ali Al Alak<sup>3</sup> · Asala H. Ali<sup>1</sup>

Received: 14 April 2019 / Accepted: 22 June 2019 / Published online: 27 June 2019  
© Springer Science+Business Media, LLC, part of Springer Nature 2019

## Abstract

Transparent conducting Copper oxide CuO thin films were successfully synthesized on glass and n-type Silicon substrates by successive ionic layer adsorption and reaction method. The crystal structure, surface texture, optical and electrical properties were studied. The results revealed that the deposited CuO thin films at different cycles number (5, 10, 15), have polycrystalline structure nature with monoclinic phase, and the crystallite size increases with the increase of cycles number. The average roughness and the root mean square values increase with increasing cycles number. The optical energy band gap and Urbach energy was decrement from 2.33 eV and 1.2 eV for 5 cycles to 2.1 eV and 0.82 eV for 15 cycles. The electrical properties of Ni/CuO/n-Si pn junction were studied using current–voltage ( $I$ – $V$ ) measurements. The barrier heights ( $\Phi_B$ ) of Ni/CuO/n-Si thin films were calculated and its values are (0.716, 0.736, 0.723) eV, for 5, 10 and 15 cycles respectively with an applied bias voltage of 3 V.

**Keywords** CuO nanostructure · Thin films · SILAR method · Surface topography · CuO/n-Si junction

## 1 Introduction

A semiconductors pn junction plays very important roles in the newest of electronic application technology and in understanding the act mechanism of other semiconductor devices (Sze 2002; Shinde et al. 2018). Copper oxide CuO is one of the most important components of the metal oxide semiconductor, involving both IB and VIA group elements in the periodic table, where IB and VIA represent group 11 and group 16 of the periodic table of the elements (Gençyılmaz and Taskopru 2017). P-type, monoclinic structure with narrow band gap (1.2–2.1) eV at room temperature (Sahu et al. 2019; Du et al. 2019). In recent years CuO thin films attracted scientific research attention in a wide range of applications

---

✉ Adel H. Omran Alkhayatt  
adilh.alkhayat@uokufa.edu.iq

<sup>1</sup> Faculty of Science, University of Kufa, Najaf, Iraq

<sup>2</sup> Directorate of Education in Al Najaf, Ministry of Education, Najaf, Iraq

<sup>3</sup> Faculty of Engineering, University of Kufa, Najaf, Iraq

in optoelectronic and microelectronics fields such as glucose, gas and bio sensors (Cavusoglu and Aydin 2019; Han et al. 2018), solar hydrogen production, photodegradation and solar energy transformation (Chang et al. 2011), catalysis (Teng et al. 2008), batteries (Chen et al. 2019), and magnetic storage media (Gao et al. 2010). A variety of growth techniques have been used to synthesize CuO nanostructure such as sputtering (Feng et al. 2011), electrodeposition (Wang et al. 2014), thermal oxidation/physical vapor deposition (PVD) (Valladares et al. 2012), chemical vapor deposition (CVD) (Albores et al. 2012), sol–gel (Das et al. 2011), chemical bath deposition (CBD) (Bayansal et al. 2012), and successive ionic layer adsorption and reaction (SILAR) method (Taysioglu et al. 2009).

Within these techniques, the new solution method modified Chemical bath deposition (m-CBD) called SILAR method, which has many advantages such as a very simple method, low cost, deposition at low temperature, safe, environmentally friendly and suitable for large areas deposition (Cavusoglu and Aydin 2019; Kovacı et al. 2018). Moreover, SILAR method is a very easy way to adding impurities of any element to the material of the thin film, the high-quality substrates and the vacuum at any stage does not required, the cycles number and the cycle time can control the thickness of the deposited films, and different types and dimensions of substrate material can be used (Shinde et al. 2018; Taysioglu et al. 2009; Bayansal et al. 2013). The thin films growth using SILAR method takes place only heterogeneously on the solid–solution interface because of the rinsing step between the cation and anion immersions. In (m-CBD) SILAR method the main disadvantage is the formation of hydroxide phase firstly which is converted to the oxide after the annealing process (Bayansal et al. 2013). In the present work, Ni/CuO/n-Si pn junction structures were fabricated by a simple method which the semiconducting layers were deposited by SILAR method. The effect of deposition cycles number on the structure, surface texture, optical and electrical properties of CuO nanostructure thin films was investigated.

## 2 Experimental details

Copper oxide thin films have been deposited on two substrate types glass and (111) orientation n-type Si. The glass substrates were chemically cleaned in an ultrasonic bath using sulfuric acid solution  $\text{H}_2\text{SO}_4\text{:H}_2\text{O}$ , 1:5, v/v, acetone, and deionized water for 10 min for each one. Whereas the Silicon substrates were cleaned with wet chemical etching using the RCA cleaning method prior to deposition (Selman et al. 2014). In the first step, to remove organic contaminants and heavy metals from the surface a 1:1:5 by volume solution of  $\text{NH}_4\text{OH:H}_2\text{O}_2\text{:H}_2\text{O}$  was used. In the second step, to remove aluminum, magnesium, and light alkali ions a 1:1:5 by volume solution of  $\text{HCl:H}_2\text{O}_2\text{:H}_2\text{O}$  was used. Each step was performed with placid heating at 75–80 °C on a hot plate for 10 min. After each step, the wafer was rinsed with deionized (DI) water. The native oxide on the Si surface was subsequently removed in the third step. The wafer was immersed into the plastic container containing diluted HF solution ( $\text{HF:H}_2\text{O}$ , 1:50 v/v) for 20 s. The Si substrate was then directly removed from the solution and stored in DI water for 5 min. Finally, the sample was dried using nitrogen gas before deposited CuO thin films. SILAR (m-CBD) method was used for the deposited of CuO thin films on the glass and polished n-Si substrates. 0.1 M copper chloride solution was obtained by dissolved 1.7048 g of  $\text{CuCl}_2\cdot 2\text{H}_2\text{O}$  copper (II) chloride dihydrates in 100 mL of deionized water under stirring in a magnetic stirrer at room temperature for 10 min. The pH value of the solution was adjusted to 10.0 by adding dropwise aqueous ammonia ( $\text{NH}_3$  30%). The solution was heated up to 90 °C and during the experiments the temperature was kept constant. One SILAR cycle can

be described as reported previously (Ali et al. 2018; Alkhayatt and Ali 2018): (1) A previously cleaned glass and Si substrates were dipped into the solution for 20 s, (2) then it was rinsed into deionized water for another 20 s to remove large and loosely bonded ions, (3) finally the substrates were dried in hot air atmosphere (simple hair dryer can be used) for 20 s. These steps were repeated for 5, 10 and 15 times. Then the prepared samples were cleaned in the ultrasonic bath for 10 min in order to detach bigger and tightly bonded particles before the analysis. Pure Ni metal was evaporated on CuO deposited films (using shadow mask), and on the back of the Si wafer (Ohmic contact) in a vacuum system of ( $1.3 \times 10^{-5}$  mbar) using Edwards Auto 306 thermal Evaporator. The Ohmic sides (Si back sides) were covered with photo-resist to prevent the growth of CuO on it. In this way, Ni/CuO/n-Si pn junction structures were fabricated. The structural, surface texture, optical and electrical properties of the prepared samples were studied by using X'Pert Pro MPD x-ray diffractometer, AFM atomic force microscope CSP model AA3000, Mega 2100 UV-Vis spectrometer and Keithly model 2400 respectively. Moreover the thickness of the deposited films was calculated using weight method.

### 3 Results and discussion

#### 3.1 Structural studies

##### 3.1.1 X-ray diffraction

The crystal structure of the deposited films were investigated by x-ray diffraction. The X-ray diffraction patterns of CuO thin film deposited on glass substrate at different cycles number (5, 10 and 15) cycles by SILAR method are depicted in Fig. 1. The deposited CuO film at 5 cycles number reveals very low crystallinity and the crystallinity enhanced with increase of cycles number. CuO films deposited at 10 and 15 cycles number was found to have polycrystalline nature and grown in the monoclinic crystal structure and match well with JCPDS card 41-0254. It is observed that the main peaks appeared at  $2\theta = 32.5^\circ, 35.19^\circ$  and  $38.7^\circ$  which are belong to (110), (002), (111) planes, respectively. The preferred orientation is a long (002) and (111) plans at  $2\theta = 35.5^\circ$  and  $38.7^\circ$ , the intensities of these peaks increased with increase cycles number which can be attribute to the increase of films thickness where the crystallite size increase and the film crystallinity enhanced. The broadening of diffraction peaks can be attributed to the nanocrystalline nature of CuO materials. The value of the full width at half maximum FWHM decrease with increase cycles number as illustrated in Table 1. The inter planer spacing ( $d_{hkl}$ ) can be calculated using Bragg's law (Quinn and Soo Yi 2009):

$$n\lambda = 2d_{hkl} \sin \theta \quad (1)$$

The crystal phases available for CuO are monoclinic structure. Monoclinic phase is characterized by determining the (a, b, c) lattice constant from X-ray diffraction pattern using the following formula (Waseda et al. 2011):

$$\frac{1}{d_{hkl}^2} = \frac{1}{\sin^2 \beta} \left( \frac{h^2}{a^2} + \frac{k^2 \sin^2 \beta}{b^2} + \frac{l^2}{c^2} - \frac{2hl \cos \beta}{ac} \right) \quad (2)$$

The values of interplaner spacing  $d_{hkl}$  and the lattice constants was in good agreement with standard values as shown in Table 1 and they are well matching with standard values. The

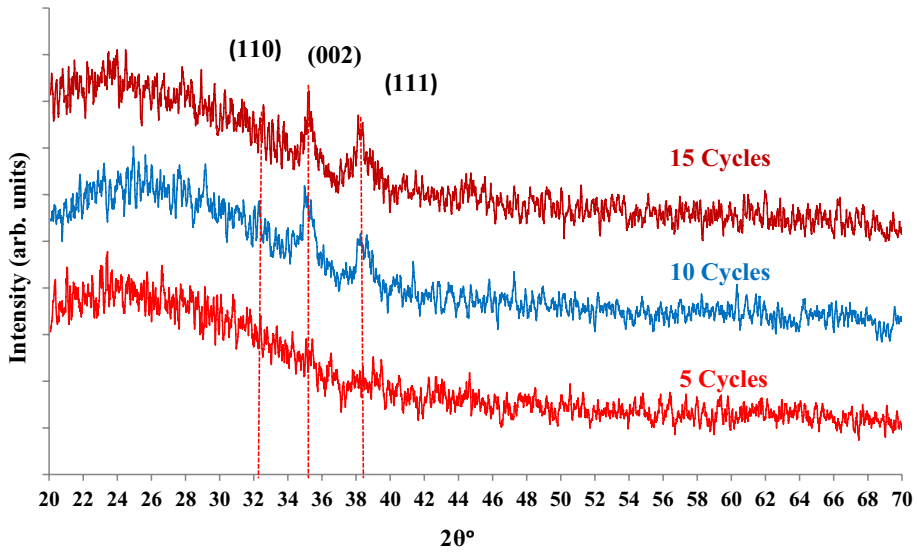


**Fig. 1** XRD patterns of CuO thin films deposited at different cycles number (5, 10, 15)

**Table 1** XRD data of CuO thin films prepared at different cycles number

Cycles number	2θ	d(Å)	d(Å)	(hkl)	a (Å)	b (Å)	C (Å)	FWHM
	Degree	Observed	Standard					
5	32.355	2.7670	2.7520	(110)	4.761	3.424	5.132	0.11
	38.751	2.3237	2.3230	(111)				1.57
10	31.996	2.7971	2.7520	(110)	4.915	3.424	5.179	0.11
	35.133	2.5543	2.5310	(002)				0.47
	38.337	2.3479	2.3230	(111)				0.94
15	32.535	2.7521	2.7520	(110)	4.688	3.421	5.171	0.11
	35.192	2.5502	2.5310	(002)				0.31
	38.209	2.3554	2.3230	(111)				0.39

crystallite size ( $D$ ) of CuO thin films was calculated from FWHM, using Scherrer's Formula (Kahraman et al. 2012):

$$D = \frac{k\lambda}{\beta \cos\theta} \quad (3)$$

where ( $k$ ) is the shape factor (0.94), ( $\lambda$ ) is the X-ray wave length, ( $\theta$ ) is Bragg angle of the diffraction peaks and ( $\beta$ ) is the FWHM in radian. The crystallite size ( $D$ ) of CuO thin films increased with increase cycles number, which can be attribute to the increase in the deposition time and film thickness, as shown in Table 2. The crystal defects such as dislocation density ( $\delta$ ) which was defined as the number of dislocation lines cross the unit area in the crystal, was determined using the formula (Callister 1997):

$$\delta = \frac{1}{D^2} \quad (4)$$

**Table 2** The thickness, crystallite size, dislocation density, no. of crystallites, micro strain and strain of CuO thin films as a function of deposited cycles number

Cycles Number For (111) plane	Film thickness (nm)	Crystallite size D (nm)	$\delta \times 10^{14} (\text{m}^{-2})$	$N \times 10^{-22} (\text{line} \cdot \text{m}^{-2})$	$\epsilon^* 10^{-3}$	Strain $\times 10^{-3}$
5	97.37	5.85	320.08	557.606	6.47	1.013
10	140.64	9.30	115.5	174.604	1.96	0.915
15	302.07	22.32	20.07	27.163	1.30	0.759

The value of dislocation density decreased with increase cycles number and it is obvious that the enhancement in the crystallinity reduce the dislocation crystal defects as illustrated in Table 2. The crystallites number (N) was determined using formula (AliYıldırım and Ateş 2010):

$$N = \frac{t}{D^3} \quad (5)$$

The value of the crystallites number (N) decrease with increase cycles number which related to the increase of crystallite size as illustrated in Table 2.

The lattice micro-strain ( $\epsilon$ ) is the percentage of deformation of the material during the growth of the film or arises from expansion or compression and can calculate from the following relation (Ashraf et al. 2011):

$$\epsilon = \frac{\beta \cos \theta}{4} \quad (6)$$

The lattice micro-strain ( $\epsilon$ ) deposited at different cycles number is found to be expansive in nature and decreased with increase cycles number. The strain represents the shift of the constant  $c_{\text{XRD}}$  value from JCPDS standard value which can be calculated by using equation (Thahab et al. 2016):

$$\text{Strain} = \left| \frac{C_{\text{XRD}} - C_{\text{ASTM}}}{C_{\text{ASTM}}} \right| \times 100\% \quad (7)$$

The value of strain at different cycles number was decreased with the increase of the cycles number as shown in Table 2.

### 3.1.2 Atomic force microscope (AFM)

Atomic force microscopes (AFM) is suitable for display images the surface topography of the deposited CuO thin films when the surface grains sizes are far below one micron. Figure 2a–c reveals the AFM images of CuO thin films deposited at different cycles number. The results showed that deposited CuO thin films exhibit variable surface texture. The obtained results of the deposited films retrieved from the possibilities on tailoring the surface texture of the CuO thin films by changing cycles number. At different cycles number, the average roughness and the root means square (RMS) values increases with the increase of cycles number as shown in Table 3. From Fig. 2 and Table 3 the RMS roughness for CuO deposited at 5 cycles number was 0.59 nm and increases to 42.5 nm with the increase of cycles number to 10 cycles. This big difference can be attributed to following, the nucleation process was began and occurred at low cycles number with a low surface

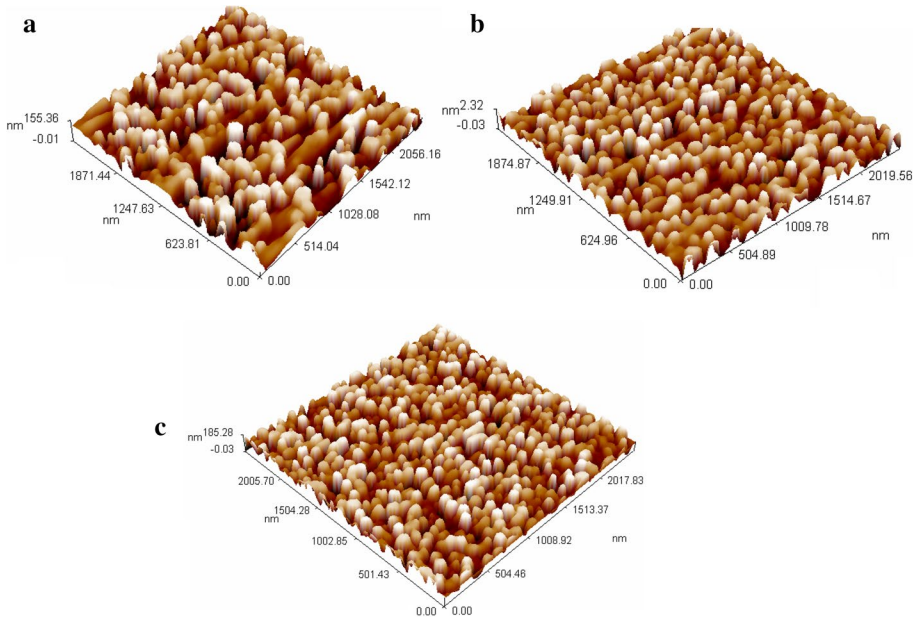


**Fig. 2** AFM Images of CuO thin film at cycles number: **a** 5 cycles, **b** 10 cycles, **c** 15 cycles

**Table 3** The average roughness, root mean square roughness and the average grain diameter of CuO thin films deposited at different cycles number

Cycles number	Roughness average (nm)	Root mean square (nm)	Avg. diameter (nm)
5	0.499	0.59	97.45
10	36.5	42.5	98.15
15	41.4	48.6	84.06

area, whereas with the increase of cycles number to 10 cycles the growth process occurred and take place with high surface area. As well as the increase in deposition cycles number lead to increase of film thickness and large grain formation with high porosity (Abdallah et al. 2018; Ganesan et al. 2019). Therefore the RMS roughness was increased and reach 48.6 at 15 cycles number.

### 3.2 Optical studies

The deposition cycles number in the SILAR method, effect on the optical characteristics of the prepared CuO films. A plot of optical transmittance of CuO films as a function cycles number in the wavelength range of 400–1000 nm was shown in Fig. 3. The film has low transmittance about 28% in the visible region (400–700) nm at cycles number more than 5 cycles whereas the film deposited at 5 cycles has the highest transmittance which about 76% in the NIR region (800–1000) nm. The transmittance was decreased gradually with an increase in deposition cycles number and increase the film thickness. The low transmittance in the visible range can be attributed to a high absorbance and the highest absorbance values are observed at

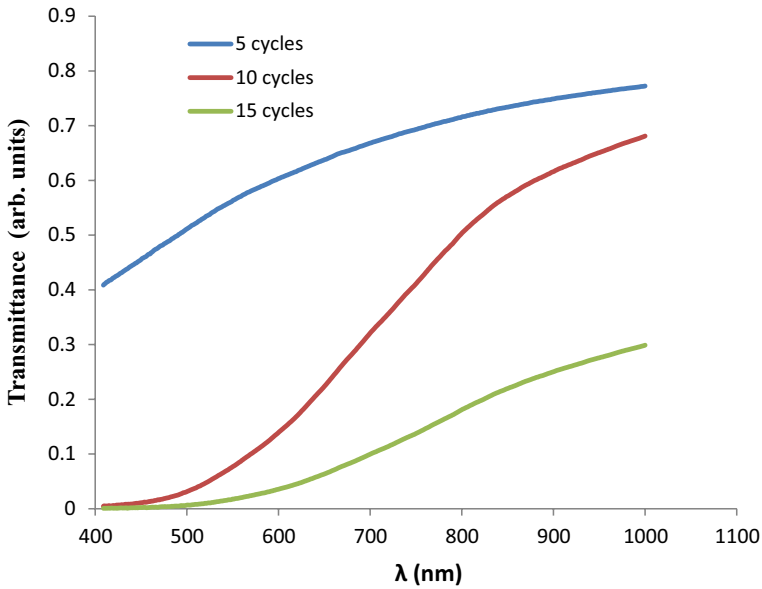


Fig. 3 Optical transmittance spectra of CuO films at different cycles number

the highest deposition cycles number and highest film thickness (Table 4). On the other hand, CuO film is suitable as an absorber layer in solar cell construction and applications (Moumen et al. 2017).

For the direct semiconductor materials the optical energy band gap  $E_g$  was calculated from the absorption spectra using Tauc relation (Polat et al. 2011):

$$(\alpha h\nu) = c(h\nu - E_g)^{1/2} \tag{8}$$

Where  $\alpha$  is the absorption coefficient,  $h\nu$  is the incident photon energy and (C) is an energy independent constant. Hence, in order to study the effect of cycles number on the optical energy band gap,  $(\alpha h\nu)^2$  is plotted versus  $(h\nu)$  as shown in Fig. 4. The linear nature of the plots indicates the present of direct transitions, at high photon energy from the obtained straight line, the direct allowed energy gap could be determined as listed in Table 4. It can be noted that  $E_g$  values of the films have a linear dependence on cycles number which mean that the increase of cycles number lead to decrease in the  $E_g$  values of prepared films from 2.33 eV for 5 cycles to 2.1 eV for 15 cycles. This can be related to the increase of the crystallite size and the enhancement in the crystallinity by increasing of film thickness which leads to increase the localized density of states with in the band gap as increase of cycles number.

In energies lower than the optical energy gap there is an absorption tails which is called Urbach energy ( $E_u$ ), such tails in films are formed mainly by volatility in bond angles and length.

In the fundamental absorption edge at the exponential region, Urbach rule can be expressed as (Alkhayatt and Hussianb 2017):

$$\alpha = \alpha_0 \exp\left(\frac{h\nu}{E_u}\right) \tag{9}$$

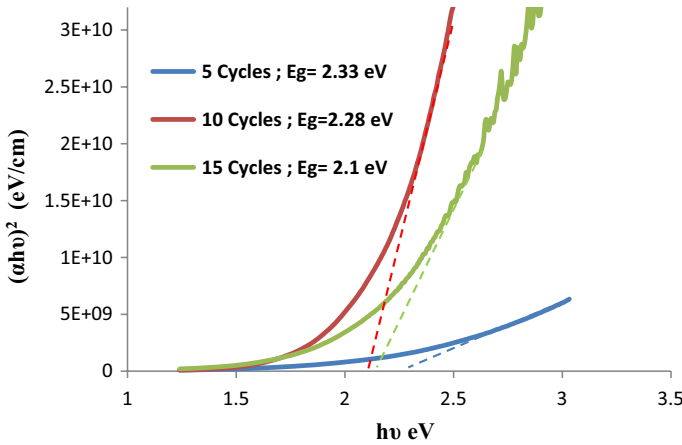


Fig. 4 Comparison of  $(\alpha hv)^2$  Versus  $(hv)$  plots of CuO thin films at cycles number (5,10,15) cycles

where  $(\alpha_0)$  is constant and  $(E_u)$  is Urbach energy, which represent the slope of the exponential region by plot the curve between  $(\ln \alpha)$  as function of  $(hv)$  (Ilica et al. 2008). This equation can describe the optical transition between the occupied valence band tails levels to the unoccupied extended levels in the conduction band edge. From Table 4 it can be seen that  $(E_u)$  decreases with the increase cycles number. Amorphous and disorder are usually related to the crystal structure defects in the material, which leads to a widening of the density of states in the band edge tails. Where the decrease in Urbach energy tails can be attribute to the decrease of density of states and the localized state within the band gap from the increase of film thickness by increase of cycles numbers (Alkhayatt and Hussianb 2017; Alkhayatta et al. 2016) (Fig. 5).

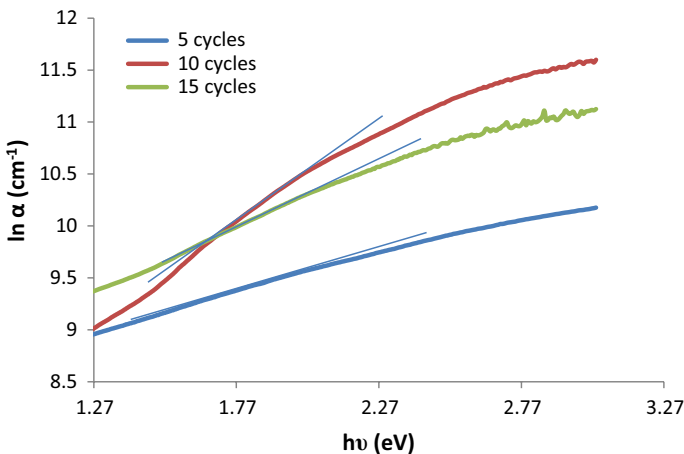


Fig. 5 Variation of  $\ln(\alpha)$  versus incident photon energy of CuO thin films with different cycles number



**Table 4** The optical properties of the CuO thin films at different cycles number

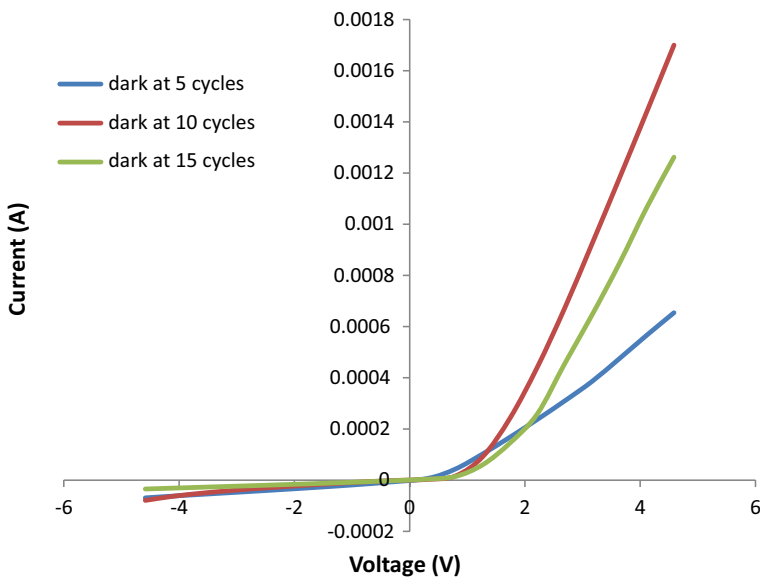
Cycles number	Thickness (nm)	Eg (eV)	Eu (eV)
5	97.37	2.33	1.2
10	239.47	2.28	0.53
15	302.07	2.1	0.82

### 3.3 Electrical studies

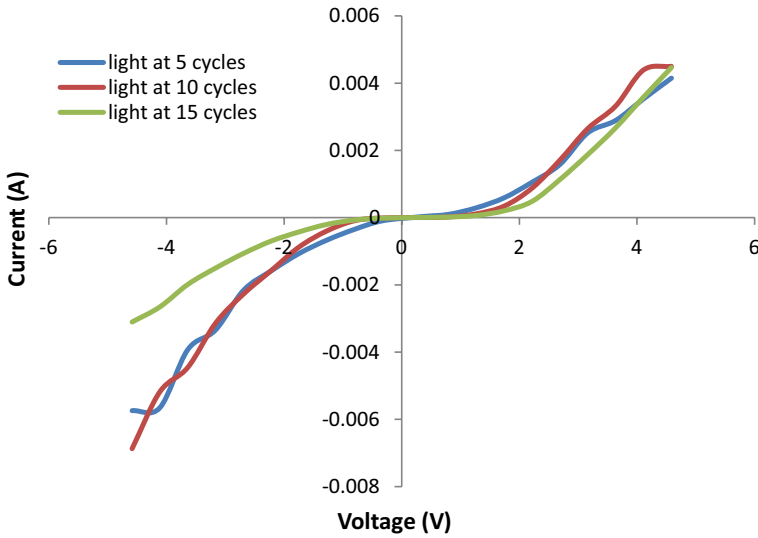
The I–V characteristics of p-CuO/n-Si hetero-junctions measured under dark current at a different cycles number were shown in Fig. 6. As shown in this figure, the reverse currents are very weak and the forward currents increase sharply with the bias voltage, the current increase with the increase cycles number and increase voltage above (1.5 to –1.5) volt becomes increasing current none gradually. This testifies that the samples show apparently a rectifying behavior, and a built-in potential is formed in all the samples.

Figure 7 shows the I–V characteristics of Ni/p-CuO/n-Si hetero-junctions measured under light current at a different cycles number. From the figure, the forward currents slightly increase and the reverse currents are not very weak, with the increase of bias voltage, the current increase with the increase of cycle number and increase voltage above (2 to –2) volt becomes increasing current un gradually. This certifies that the samples show obviously a rectifying behavior, and a built-in potential is created in all the samples.

These results can be attributed to the improvements in the crystallinity and the crystal structure of the prepared thin films which lead to a narrow energy band gap and therefore, the electrons need lower energy to traverse the band gap so, it can be noted that the photo-current be higher after increasing cycles number.



**Fig. 6** I–V characteristics under dark for CuO/Si heterojunction at forward and reverse bias voltage at different cycles number



**Fig. 7** I–V characteristics under light for CuO/Si heterojunction at forward and reverse bias voltage at different cycles number

Schottky barrier height was specified from I–V characteristics, for thermionic emission and ( $V > 3k_B T/q$ ), the general diode equations are as follow (Akosoy et al. 2010; Sze 1989):

$$I = I_o \exp \left[ \frac{qV}{(nk_B T)} \right] \tag{10}$$

$$I_o = A^* A T^2 \exp \left[ \frac{-q\Phi_B}{(k_B T)} \right] \tag{11}$$

Where ( $I_o$ ): saturation current, (n): ideality factor, ( $k_B$ ): Boltzmann constant, (T): absolute temperature, ( $\Phi_B$ ): barrier height, (A): area of the Schottky contact and ( $A^*$ ): effective Richardson coefficient. The theoretical value of ( $A^*$ ) can be calculated using the following equation (Abud 2014; Ng 1995):

$$A^* = \frac{4\pi m^* q k_B^2}{h^3} \tag{12}$$

where (h): Planck constants, ( $m^* \sim 7.9m_o$ ) is the effective hole mass.

The plot of  $\ln I$  versus  $V$  showed a straight line, and ( $I_o$ ) is determined from the intercept with  $\ln I$  (y-axis) as shown in Fig. 8. It was found that the barrier height for Ni/CuO/Si was increased with increase cycles number and has a lower value 0.716 eV at 5 cycle as compared to that of Ni/CuO/Si deposited at 10 cycles 0.736 eV and at 15 cycles 0.723 eV. This can be attributed to the fine surface texture of CuO thin film deposited on Si substrate and the impact of the Si substrate background conductivity on the surface

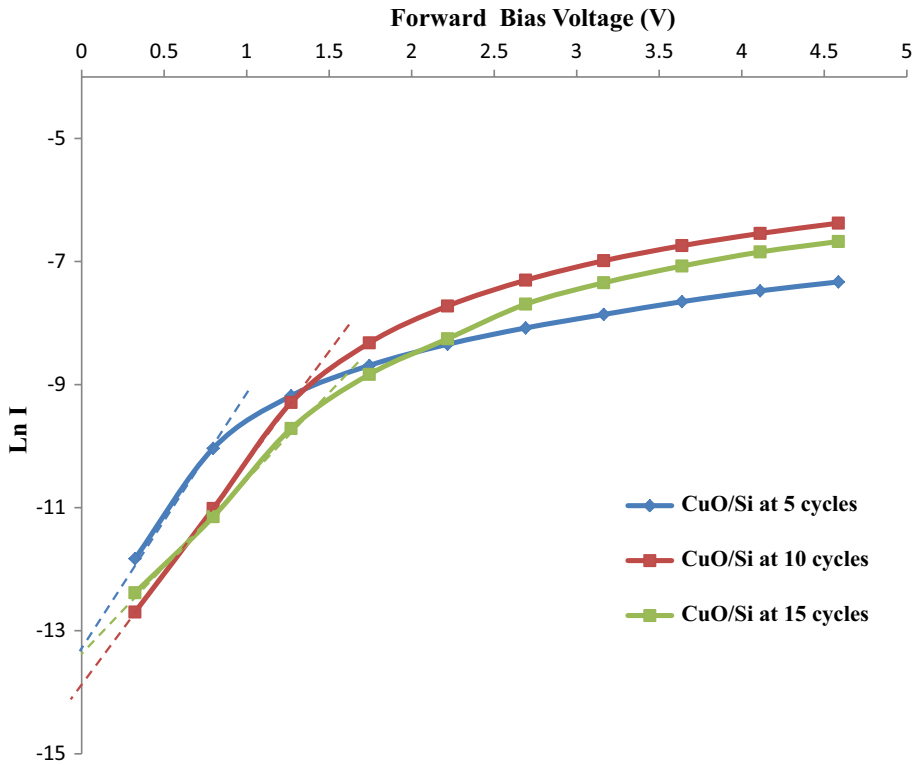


**Fig. 8**  $\ln I$  versus  $V$  for forward bias of dark for the prepared p-CuO/n-Si heterojunction at 5, 10 and 15 cycles

**Table 5**  $\eta$ ,  $\gamma$ ,  $\Phi_B$  and  $I_s$  values of CuO/Si heterojunction

Ni/CuO/Si at	$\eta$	$\gamma (V)^{-1}$	$\Phi_B$	$I_s (\mu A)$
5 cycles	1.62	0.427	0.716	2.17
10 cycles	1.69	0.558	0.736	0.97
15 cycles	2.22	0.647	0.723	1.61

sheet resistivity of CuO film which leads to enhancement the CuO–Ni thin film-metal interface properties after the increase of deposition cycles number (Table 5).

### 4 Conclusion

In this work, Ni/CuO/n-Si pn junction was synthesized by SILAR method. The crystal structure, surface texture and optical characteristics of CuO thin films, as well as the junction electronic parameters, were studied as a function of cycles number (5, 10 and 15). The crystallinity was enhanced and the crystallite size ( $D$ ) increase, with increase cycles number with less dislocation density and crystal defects. Whereas the transmittance and the absorption edge red shifted. The optical band gap ( $E_g$ ) and Urbach energy ( $E_u$ ) decrease

with increase of cycles number, so the prepared films was suitable material for preparation of solar cells and other optoelectronic devices. Smooth surface texture and the average roughness were increase with increase cycles number. I–V characteristics revealed the lower barrier height on Ni/CuO/n–Si pn junction at 5cycles and increase with the increase of deposition cycles. These results related to the improvement of CuO/Si thin films interfaces with Ni contact surface. The results reveal that the low-cost SILAR technique is a suitable method for deposited CuO thin film.

**Acknowledgements** The authors would like to acknowledge the department of physics in faculty of science, university of Kufa/Iraq, Dr. Mazin Aunay Mahdi Department of Physics in college of Science, University of Basrah, and NAMRU in Faculty of Engineering/University of Kufa/Iraq.

## References

- Abdallah, B., Ismail, A., Kashoua, H., Zetoun, W.: Effects of deposition time on the morphology, structure, and optical properties of PbS thin films prepared by chemical bath deposition. *Hindawi J. Nanomater.* **2018**, 1–8 (2018). <https://doi.org/10.1155/2018/1826959>
- Abud, S.H.: Porous In<sub>x</sub>Ga<sub>(1-x)</sub>N for Sensing and Solar Cell Application, PhD. Thesis University Penang-Malaysia (2014)
- Akosoy, S., Caglar, Y., Ilıcan, S., Caglar, M.: Effect of Sn dopants on the optical and electrical properties of ZnO films. *Optica Applicata* **40**(1), 7–14 (2010)
- Albores, F.P., Flores, W.A., Madrid, P.A., Valdovinos, E.R., Zapata, M.V., Delgado, F.P., Yoshida, M.M.: Growth and microstructural study of CuO covered ZnO nanorods. *J. Cryst. Growth* **351**, 77–82 (2012)
- Ali, A.H., Al-Fatlawi, I.J., Ressen, A.H., Alkhayatt, A.H.O.: Influence of solution pH and NH<sub>3</sub> concentration on some properties of CuO thin films deposited by chemical solution method. *J. Eng. Appl. Sci.* **13**(23), 9961–9967 (2018)
- AliYıldırım, M., Ateş, A.: Influence of films thickness and structure on the photo-response of ZnO films. *Opt. Commun.* **283**, 1370–1377 (2010)
- Alkhayatt, A.H.O., Ali, A.H.: Influence of cycles number and time on the structural, surface morphology and some optical properties of CuO nanostructure thin film prepared by SILAR method. *Sensor Lett.* **16**, 64–70 (2018)
- Alkhayatt, A.H.O., Hussianb, S.K.: Fluorine dopant concentration effect on the structural and optical properties of spray deposited nanocrystalline ZnO thin films. *Surfaces Interfaces* **8**, 176–181 (2017)
- Alkhayatta, A.H.O., Thahabb, S.M., Zgairaa, I.A.: Structure, surface morphology and optical properties of post-annealed delafossite CuFeO<sub>2</sub> thin films. *Optik* **127**, 3745–3749 (2016)
- Ashraf, M., Akhtar, S.M.J., Khan, A.F., Ali, Z., Qayyum, A.: Effect of annealing on structural and optoelectronic properties of nanostructured ZnSe thin films. *J. Alloys Compd.* **509**, 2414–2419 (2011)
- Bayansal, F., Çetinkara, H.A., Kahraman, S., Çakmak, H.M., Güder, H.S.: Nano-structured CuO films prepared by simple solution methods: plate-like, needle-like and network-like architectures. *Ceram. Int.* **38**, 1859–1866 (2012)
- Bayansal, F., Sahin, B., Yüksel, M., Biyikli, N., Çetinkara, H.A., Güder, H.S.: Influence of coumarin as an additive on CuO nanostructures prepared by successive ionic layer adsorption and reaction (SILAR) method. *J. Alloys Compd.* **566**, 78–82 (2013)
- Callister, W.D.: *Materials Science and Engineering—An Introduction*, pp. 174–207. Wiley, New York (1997)
- Cavusoglu, H., Aydin, R.: Complexing agent triethanolamine mediated synthesis of nanocrystalline CuO thin films at room temperature via SILAR technique. *Superlattices Microstruct.* **128**, 37–47 (2019)
- Chang, H., Kao, M.J., Cho, K.C., Chen, S.L., Chu, K.H., Chen, C.C.: Integration of CuO thin films and dye-sensitized solar cells for thermoelectric generators. *Curr. Appl. Phys.* **11**(4), S19–S22 (2011)
- Chen, W., Zhang, H., Yang, B., Li, B., Li, Z.: Characterization of Cu<sub>3</sub>N/CuO thin films derived from annealed Cu<sub>3</sub>N for electrode application in Li-ion batteries. *Thin Solid Films* **672**, 157–164 (2019)
- Das, S., Majumdar, S., Giri, S.: Room temperature weak ferromagnetism and magnetoconductance in functional CuO film. *Appl. Surf. Sci.* **257**, 10775–10779 (2011)
- Du, Y., Gao, X., Meng, X.: Preparation and characterization of single-phased n-type CuO film by DC magnetron sputtering. *Physica B* **560**, 37–40 (2019)

- Feng, J.K., Xia, H., Lai, M.O., Lu, L.: Electrochemical performance of CuO nanocrystal film fabricated by room temperature sputtering. *Mater. Res. Bull.* **46**, 424–427 (2011)
- Ganesan, K.P., Sivakumar, G., Anandhan, N., Marimuthu, T., Panneerselvam, R., Amali Roselin, A.: Influence of bath temperatures on physical and electrical properties of potentiostatically deposited Cu<sub>2</sub>O thin films for heterojunction solar cell applications. *Opt. Quant. Electron.* **51**, 37 (2019). <https://doi.org/10.1007/s11082-019-1745-8>
- Gao, W., Yang, S., Yang, S., Lv, L., Du, Y.: Synthesis and magnetic properties of Mn doped CuO nanowires. *Phys. Lett. A* **375**(2), 180–182 (2010)
- Gençyılmaz, O., Taskoprü, T.: Effect of pH on the synthesis of CuO films by SILAR method. *J. Alloys Compd.* **695**, 1205–1212 (2017)
- Han, C., Chena, X., Liu, D., Zhou, P., Zhao, S., Bi, H., Meng, D., Wei, D., Shen, Y.: Fabrication of shrub-like CuO porous films by a top-down method for high-performance ethanol gas sensor. *Vacuum* **157**, 332–339 (2018)
- Ilica, S., Caglar, Y., Caglar, M., Demirci, B.: Polycrystalline indium-doped ZnO thin films: preparation and characterization. *J. Optoelectron. Adv. Mater.* **10**, 2592–2598 (2008)
- Kahraman, S., Bayansal, F., Çetinkara, H.A., Çakmak, H.M., Güder, H.S.: Characterization of CBD grown ZnO films with high c-axis orientation. *Mater. Chem. Phys.* **134**(2012), 1036–1041 (2012)
- Kovacı, H., Akaltun, Y., Yetim, A.F., Uzun, Y., Çelika, A.: Investigation of the usage possibility of CuO and CuS thin films produced by successive ionic layer adsorption and reaction (SILAR) as solid lubricant. *Surf. Coat. Technol.* **344**, 522–527 (2018)
- Moumen, A., Hartiti, B., Thevenin, P., Siadat, M.: Synthesis and characterization of CuO thin films grown by chemical spray pyrolysis. *Opt. Quant. Electron.* **49**, 70 (2017). <https://doi.org/10.1007/s11082-017-0910-1>
- Ng, K.: Kwok, Complete guide to Semiconductor devices. AT & T Bell Laboratories, Murray Hill (1995)
- Polat, I., Aksu, S., Altunbas, M., Yılmaz, S., Bacaksız, E.: The influence of diffusion temperature on the structural, optical and magnetic properties of manganese-doped zinc oxysulfide thin films. *J. Solid State Chem.* **184**, 2683–2689 (2011)
- Quinn, J.J., Soo Yi, K.: Solid State Physics Principles and Modern Applications. Springer, Berlin (2009)
- Sahu, K., Choudhary, S., Khan, S.A., Pandey, A., Mohapatra, S.: Thermal evolution of morphological, structural, optical and photocatalytic properties of CuO thin films. *Nano-Struct. Nano-Objects* **17**, 92–102 (2019)
- Selman, A.M., Hassan, Z., Husham, M.: Structural and photoluminescence studies of rutile TiO<sub>2</sub> nanorods prepared by chemical bath deposition method on Si substrates at different pH values. *Measurement* **56**, 155–162 (2014)
- Shinde, S.K., Kim, D.Y., Ghodake, G.S., Maile, N.C., Kadam, A.A., Lee, D.S., Rath, M.C., Fulari, V.J.: Morphological enhancement to CuO nanostructures by electron beam irradiation for biocompatibility and electrochemical performance. *Ultrason. Sonochem.* **40**, 314–322 (2018)
- Sze, S.M.: Physics of Semiconductor Devices, 2nd edn. Wiley, New York (1989)
- Sze, S.M.: Semiconductor Devices Physics and Technology, 2nd edn. Wiley, New York (2002)
- Taysioglu, A.A., Peksoz, A., Kaya, Y., Derebasi, N., Irez, G., Kaynak, G.: GMI effect in CuO coated Co-based amorphous ribbons. *J. Alloys. Comp.* **487**, 38–41 (2009)
- Teng, F., Yao, W., Zheng, Y., Ma, Y., Teng, Y., Xu, T., Liang, S., Zhu, Y.: Synthesis of flower-like CuO nanostructures as a sensitive sensor for catalysis. *Sens. Actuators B* **134**, 761–768 (2008)
- Thahab, S.M., Alkhayatt, A.H.O., Zgair, I.A.: Influences of post-annealing temperature on the structural and electrical properties of mixed oxides (CuFeO<sub>2</sub> and CuFe<sub>2</sub>O<sub>4</sub>) thin films prepared by spray pyrolysis technique. *Mater. Sci. Semicond. Process.* **41**, 436–440 (2016)
- Valladares, L.D.L.S., Salinas, D.H., Dominguez, A.B., Najarro, D.A., Khondaker, S.I., Mitrelias, T., Barnes, C.H.W., Aguiar, J.A., Majima, Y.: Crystallization and electrical resistivity of Cu<sub>2</sub>O and CuO obtained by thermal oxidation of Cu thin films on SiO<sub>2</sub>/Si substrates. *Thin Solid Films* **520**, 6368–6374 (2012)
- Wang, Y., Jiang, T., Meng, D., Yang, J., Li, Y., Ma, Q., Han, J.: Fabrication of nanostructured CuO films by electrodeposition and their photocatalytic properties. *Appl. Surf. Sci.* **317**, 414–421 (2014)
- Waseda, Y., Shinoda, K., Matsubara, E.: XRD Diffraction Crystallography. Springer, Heidelberg (2011)